JMEPEG (2010) 19:1116–1127
DOI: 10.1007/s11665-010-9596-2

1059-9495/$19.00

Multidisciplinary Design Optimization for Glass-Fiber Epoxy-Matrix Composite 5 MW Horizontal-Axis Wind-Turbine Blades

M. Grujicic, G. Arakere, B. Pandurangan, V. Sellappan, A. Vallejo, and M. Ozen

(Submitted December 7, 2009)

A multi-disciplinary design-optimization procedure has been introduced and used for the development of cost-effective glass-fiber reinforced epoxy-matrix composite 5 MW horizontal-axis wind-turbine (HAWT) blades. The turbine-blade cost-effectiveness has been defined using the cost of energy (CoE), i.e., a ratio of the three-blade HAWT rotor development/fabrication cost and the associated annual energy production. To assess the annual energy production as a function of the blade design and operating conditions, an aerodynamics-based computational analysis had to be employed. As far as the turbine blade cost is concerned, it is assessed for a given aerodynamic design by separately computing the blade mass and the associated blade-mass/size-dependent production cost. For each aerodynamic design analyzed, a structural finite element-based and a post-processing life-cycle assessment analyses were employed in order to determine a minimal blade mass which ensures that the functional requirements pertaining to the quasi-static strength of the blade, fatigue-controlled blade durability and blade stiffness are satisfied. To determine the turbine-blade production cost (for the currently prevailing fabrication process, the wet lay-up) available data regarding the industry manufacturing experience were combined with the attendant blade mass, surface area, and the duration of the assumed production run. The work clearly revealed the challenges associated with simultaneously satisfying the strength, durability and stiffness requirements while maintaining a high level of wind-energy capture efficiency and a lower production cost.

Keywords design optimization, fatigue-life assessment, horizontal axis wind turbine blades

1. Introduction

The depletion of fossil-fuel reserves, stricter environmental regulations and the world's ever-growing energy needs have led to deployment/utilization of various alternative/renewable energy sources. Among the various renewable energy alternatives, wind energy is one of the most promising and the fastest growing installed alternative-energy production technologies. In fact, it is anticipated that by 2030, at least 20% of the U.S. energy needs will be met by various onshore and offshore wind-farms (a collection of wind turbines at the same location) (Ref 1).

Wind turbine is essentially a converter of wind energy into electrical energy. This energy conversion is based on the principle of having the wind drive a rotor, thereby transferring a power of

$$P = \alpha\beta\rho A v^3 \quad \text{(Eq 1)}$$

to the electrical generator, where α is an aerodynamic efficiency parameter, β is a drive-train efficiency parameter, ρ is air density, A rotor swept-surface area and v the wind speed. The P/A ratio is commonly referred to as the *specific-power rating*. To attain rotor stability and a high value of aerodynamic efficiency, α, the rotor is usually constructed as a set of three aerodynamically shaped blades. The blades are (typically) attached to a horizontal hub (which is connected to the rotor of the electrical generator, via a gearbox/drive-train system, housed within the nacelle). The rotor/hub/nacelle assembly is placed on a tower and the resulting wind energy converter is referred to as the horizontal axis wind turbine (HAWT). A photograph of an offshore wind turbine is provided in Fig. 1. All major components of the turbine are labeled for identification.

To reduce the energy production cost (typically expressed in $/kW·h), commercial wind turbines have grown considerably in size over the last 30 years (Fig. 2). The large wind-turbine economics is based on the fact that as the hub-height/rotor radius increases the average wind speed/wind energy captured increases due to the so called *wind shear* effect (a natural increase in the wind speed with elevation with respect to the terrain). Consequently, for the same energy production level, lesser number of wind turbine units are required, which in turn leads to a reduction in the cost of operation of the farm. As depicted in Fig. 2, the largest wind turbine unit currently in

M. Grujicic, G. Arakere, and **B. Pandurangan**, Department of Mechanical Engineering, Clemson University, 241 Engineering Innovation Building, Clemson, SC 29634-0921; and **V. Sellappan, A. Vallejo,** and **M. Ozen**, Ozen Engineering, Inc., 1210 E. Arques Avenue, Suite 207, Sunnyvale, CA 94085. Contact e-mails: mica.grujicic@ces.clemson.edu and mica@ces.clemson.edu.

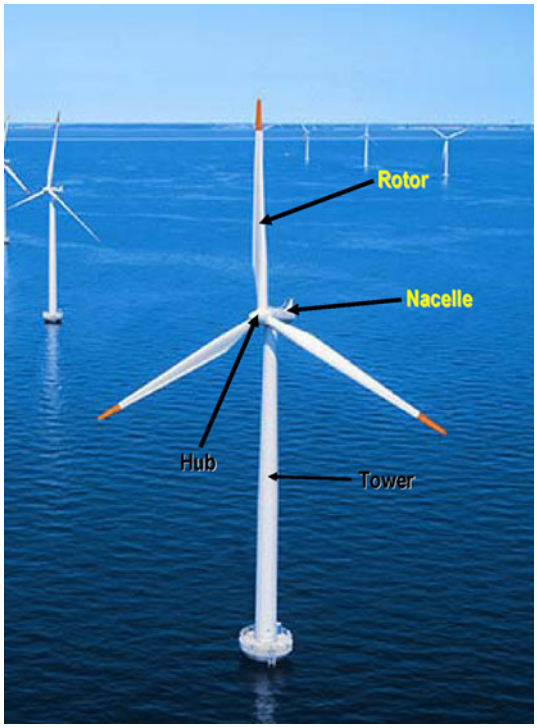

Fig. 1 Typical off-shore wind farm. The major wind turbine subsystems are identified

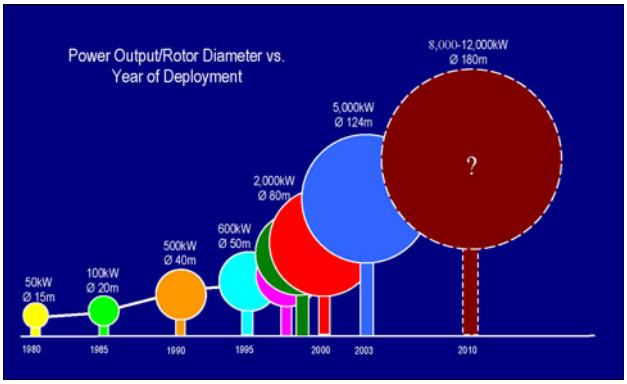

Fig. 2 Variation of the horizontal-axis wind turbine power output and rotor diameter with the year of deployment

service is rated at 5 MW and has a rotor diameter of 124 m. As the size of the wind turbine rotor increases, the structural performance, durability and dynamic-stability requirements tend to become more and more challenging to meet and it is, at present, not clear what is the ultimate rotor diameter which can be attained with the present material/manufacturing technologies. These challenges are further compounded by the concurrent requirements for high aerodynamic efficiency (as quantified by the fraction of wind energy captured by the rotor) for the rotor.

The two main structural performance requirements for wind-turbines are:

(a) Sufficient "*flap-wise*" bending strength to withstand highly-rare extreme static-loading conditions (e.g., 50-year return-period gust, a short strong blast of wind). Flap-wise bending is blade bending in a direction normal to the rotor plane of rotation caused by the wind acting mainly over the broad faces of the blade.

(b) Sufficient turbine blade "*flap-wise*" bending stiffness in order to ensure that a minimal clearance is maintained between blade tip and the turbine tower at all times during wind turbine operation.

The durability requirement for the turbine blades is typically defined as a minimum of 20-year fatigue life (which corresponds roughly to ca. 10^8 cycles) when subjected to stochastic wind-loading conditions and cyclic gravity-induced edge-wise bending loads in the presence of thermally fluctuating and environmentally challenging conditions. Edge-wise bending is blade bending in a direction parallel to the rotor plane of rotation.

Various structural/dynamics requirements are all related to a high mass of the wind-turbine blades (ca. 18 tons in the case of the 62 m long/5 MW turbine blade). This is caused by the fact that not only the blade-root and the turbine-hub to which the blades are attached need to sustain the wind and gravity-induced forces/moments accompanying the turning of the rotor, but also the nacelle (i.e. the structure that houses all of the gear boxes and the drive train connecting the hub to the power generator), the tower and the foundations must be able to withstand the whole wind-turbine dynamics.

The aforementioned structural performance, durability and structural-dynamics requirements must be met by the wind turbine rotor while ensuring a high level of aerodynamic efficiency. The primary figure of merit for aerodynamic performance of a wind turbine rotor is the annual energy production (AEP).

When considering the wind turbine rotor economics, one typically uses the so-called "*Cost of Energy*" (CoE), i.e., the rotor cost per unit energy produced either annually or over the life of the wind turbine, as the figure of merit. When calculating CoE, the required information includes the rotor/blade mass, unit-mass material/production cost and AEP. This information can be obtained in the following manner:

(a) The minimal blade mass is determined by ensuring that the aforementioned structural performance, durability and structural dynamics requirements are all satisfied.

(b) The unit-mass blade cost is a function of the material(s) used and the blade-fabrication process employed. While in a number of recently erected wind turbines glass/carbon hybrid reinforced polymer matrix composites were used (Ref 2), glass-fiber reinforced epoxy-matrix composites are still preferred. This is mainly due to a lower material cost and a relatively vast experience associated with handling and fabrication technologies employing this class of materials. Consequently, the HAWT blades analyzed in the present work will be assumed to be made of conventional glass-fiber reinforced epoxy-matrix composites with the composite-material architecture varied throughout the blade to best meet the local load-bearing/transfer needs.

(c) In regard to the HAWT-blade manufacturing cost, one must first identify the fabrication technology employed. While four major HAWT-blade fabrication technologies (i.e., the wet lay-up, the prepreg, the resin-infusion and the filament-winding) have been employed over the last

30 years, the traditional open-mode wet lay-up technology is still the most prevalent (Ref 3). Consequently, the blades analyzed in the present work will be assumed to have been fabricated using this technology and their fabrication cost will be then assessed using the available industry-based open-literature data (Ref 4).

(d) As stated above, the annual energy production can be determined using the appropriate aerodynamics-based wind-rotor interaction analysis.

(e) Finally, once the rotor/blade material/fabrication cost and the AEP are determined, the corresponding CoE can be readily calculated as a ratio of the two.

A review of the literature carried out as part of the present work clearly revealed that the development and construction of highly reliable large rotor-diameter wind turbines is a major challenge since wind turbines are large, flexible, articulated structures subjected to stochastic transient aerodynamic loading conditions. It is, hence, not surprising that several wind-turbine manufacturers face serious problems in meeting the structural performance, durability and structural dynamics requirements. The inability to meet the aforementioned requirements is often caused by failure of the transmission gear pinions, failure of bearings, blade fracture, tower buckling, etc. When these problems persist, insurance companies become reluctant in providing their services to the wind-turbine manufacturers causing production shut-down and often company bankruptcy. In order to help prevent these dire consequences, more and more wind-turbine manufacturers are resorting to the use of advanced computer-aided engineering tools, during design, development, verification and fabrication of their products.

Turbine blades and the drive-train are perhaps the most critical components/subsystems in the present designs of wind turbines. The present work deals only with the issues related to the performance, reliability and cost of HAWT blades. In Fig. 3(a), a typical cross-section of a HAWT-blade is displayed and the major components are labeled. A typical HAWT-blade planform, i.e., the variation of the chord length along the blade length, is shown in Fig. 3(b). As seen in Fig. 3(a), the aerodynamic shape of the blade is obtained through the use of separately fabricated and adhesively joined outer shells (often referred to as the *outer skin* or the upper and lower *cambers*). While the outer skins provide the required aerodynamic shape, an internal box-like beam running down the length of the blade is used to obtain the necessary structural and durability performance of the blade. The vertical sides of the box-shaped beam are normally referred to as *shear webs* since their role is to provide a shear-type coupling between the upper and lower sides of the beam (the upper and lower *spar caps*). Since the main role of the spar caps is to provide the necessary flap-wise and edge-wise bending load bearing capacity, their thickness is typically large in comparison to those of the shear webs and the outer shells. Consequently, spar caps make a major contribution to the overall mass of a HAWT blade.

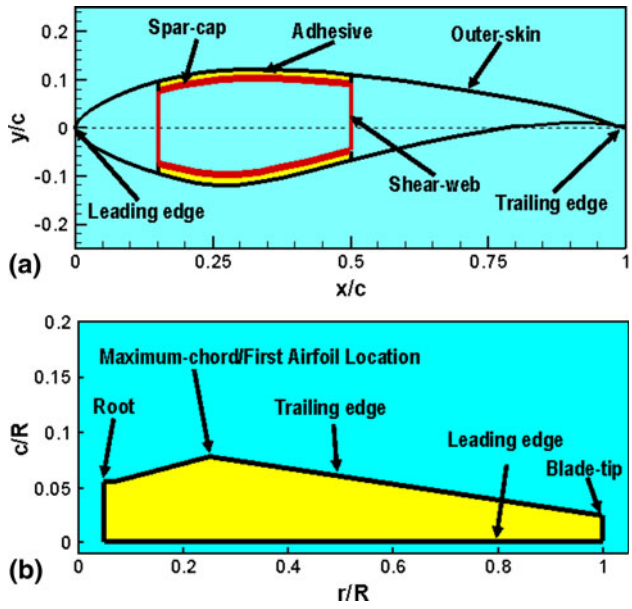

Fig. 3 (a) A typical HAWT blade cross-section and (b) the corresponding planform

The main objective of the present work is to develop a multi-disciplinary design-optimization procedure and demonstrate its utility using the case of a glass-fiber reinforced epoxy-matrix composite 5 MW HAWT blade. It is hoped that the present approach will help widen the use of the computer-aided engineering (CAE) tools in the area of HAWT-blades design/development so that many critical decisions regarding the design and fabrication of these components can be made in the earlier stages of the overall design cycle. This strategy has been proved to yield very attractive economic benefits in the case of more mature industries such as the automotive and the aerospace industries (Ref 5).

The organization of the paper is as follows. A brief overview of the approach used for automated HAWT-blade geometrical model and the full finite-element input deck generation is presented in Sect 2.1. A brief description of the HAWT blade multidisciplinary design optimization procedure along with the associated aerodynamics, structural, durability and cost analyses is given in Sect 2.2. The results obtained are presented and discussed in Sect 3. The key conclusions resulting from the present work are summarized in Sect 4.

2. Computational Procedures

2.1 Geometrical and Meshed Models

The wind-turbine blade is essentially a cantilever beam mounted on a rotating hub. The aerodynamic shape of the blade is formed by relatively thin outer shells. The loads acting on the blade are mainly supported by a longitudinal box-shaped spar. To reduce the maximum bending moments located at the blade root (the section where the blade is attached to the hub), wind-turbine blades are generally tapered along the span. Tapering typically includes not only the blade cross section chord and thickness but also the thicknesses of the outer shells, spar caps and shear webs. This ensures that different blade sections experience comparable extreme loading (e.g. the maximum strain), so that no unnecessary local over-sizing is present. In addition to the taper, turbine blade generally possess a certain amount of twist along their length. Twist is beneficial with respect to lowering the torque required for self-starting of the rotor and for the attainment of the optimal effective wind attack angle during the wind turbine operation.

The geometrical and the meshed finite-element models for the 5 MW HAWT blades analyzed in the present work were

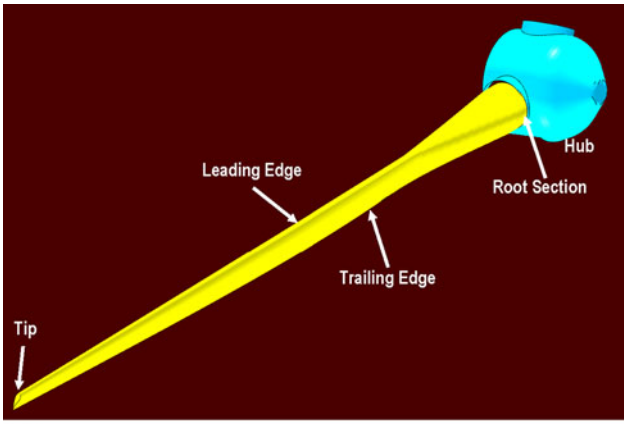

(a)

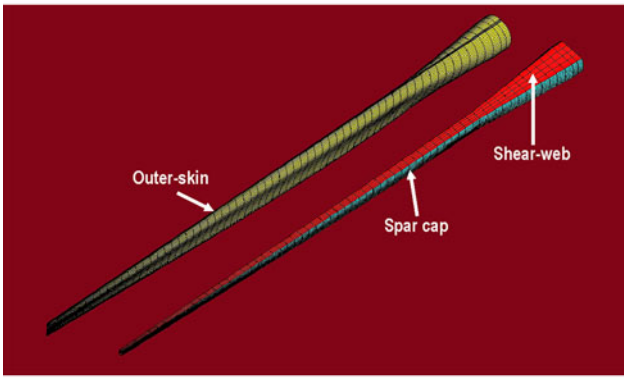

(b)

Fig. 4 Typical (a) geometrical and (b) meshed models of a single wind-turbine blade analyzed in the present work

generated using a MATLAB (Ref 6) based computer program described in our recent work (Ref 7). The program enables the creation of the entire wind-turbine blade geometrical model (in the .stl format) and a finite-element mesh model (for a given set of parameters related to the taper, twist, shear-web lateral positions, mesh-topology, etc.).

Examples of the wind-turbine blade geometrical model and of the corresponding finite-element meshed model are displayed respectively in Fig. 4(a) and (b).

As mentioned earlier, the case of a prototypical 5 MW HAWT with a 60 m rotor radius and a specific power rating (a ratio of the power rating to the rotor swept area) of 0.44 kW/m^2 was considered in the present work. Design optimization of the blades in this turbine for cost-effective energy production is analyzed.

2.1.1 Geometrical Model. While the blade shape and dimensions are varied in the course of their design optimization, the prototypical blade dimensions/geometrical parameters were as follows: (a) blade diameter at the root = 3.23 m; (b) chord length at the first airfoil station located at 25% span = 4.57 m; (c) chord length at the blade tip = 1.66 m (with a linear taper in-between); (d) S818 airfoil shape; and (e) the following twist angle schedule: 10° at 25% span, 2.5° at 50% span, 0° at 75% span and −0.5° at the blade tip.

2.1.2 Meshed Model. A typical finite-element meshed model was constructed as follows: (a) the outer skins and the shear webs are composite shell structures and meshed using ca. 5000 and 800 first-order four-node composite-shell elements, respectively; (b) the two spar caps having a considerably larger thickness are modeled as solids and meshed using ca. 2000 first-order eight-node hexahedral solid elements; and (c) the adhesive layers joining the spar caps to the outer skins are modeled as interfacial structures and meshed using ca. 1200 eight-node traction-separation-based cohesive elements. To facilitate optimization of the HAWT-blade composite-laminate lay-up, all the meshes used were of a structured character.

It should be noted that the aforementioned geometry/mesh generator program also enabled an automated generation of the entire finite-element input deck for a selected set of parameters which is a critical requirement for efficient computer-based design-of-experiments and design-optimization analyses. For example, lateral/transverse locations of the two shear webs and the thicknesses of two spar-caps could be readily varied.

2.2 Multidisciplinary Design Optimization of a 5 MW HAWT Blade

As explained earlier, the main objective of the present work was to develop a multidisciplinary design optimization procedure and apply it to a 5 MW HAWT blade whose design is to be optimized with respect to the attainment of a minimal CoE. The multidisciplinary character of this procedure stems from the fact that different types of engineering analyses had to be employed in determining the CoE for a given design of the blade. Specifically, an aerodynamics-based procedure had to be applied in order to compute the AEP and wind-based loading while a structural performance and a durability analysis had to be employed in order to determine the minimal blade mass which ensures that all the structural and durability requirements for the blade are met. In addition, a cost estimation analysis had to be utilized before the CoE could be determined.

The design optimization procedure developed in the present work is based on a two-level optimization scheme. A flow chart showing the data flow during the optimization process is depicted in Fig. 5. Within the outer-level optimization loop, the CoE (i.e., the objective function) is being minimized with respect to a number of design variables (chord lengths and twist angles) which define the blade plan-form and the corresponding twist-angle schedule. For a given blade design at each iteration step, evaluation of the CoE requires the knowledge of the corresponding blade material/production cost and the AEP. Since the AEP is directly related to the HAWT-blade aerodynamic shape and is not dependent on the internal blade structure/architecture, the AEP is evaluated within the outer-level optimization loop. On the other hand, the blade material/production cost depends on the minimal mass of the blade which can ensure that all the structural and durability requirements of the blade are satisfied. Hence, before the material/production cost for a given blade aerodynamic design can be determined, an inner-level optimization procedure has to be employed to determine the minimal blade mass.

As seen in Fig. 5, this entails the employment of a finite-element structural analysis and a post-processing fatigue-based durability analysis. To do that, however, one must provide the wind-based loading function associated with a given blade aerodynamic design. Such loading function is determined within the outer-level optimization loop by employing the appropriate aerodynamic analysis.

Within the inner-level optimization loop, the variation of the spar cap thickness along the span (spar caps are most likely to fail when subjected to flap-wise bending loads) and

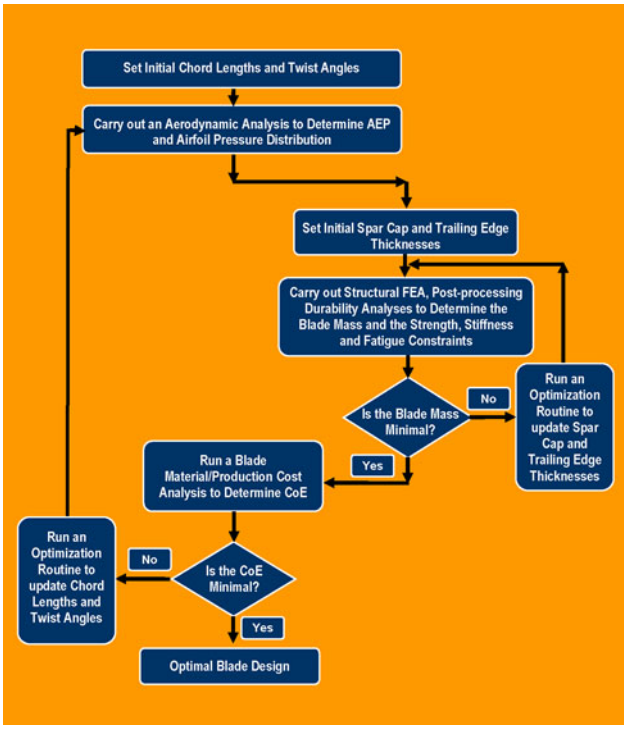

Fig. 5 A flow chart for the two-level multidisciplinary design optimization procedure for cost-effective 5 MW HAWT blade developed in the present work

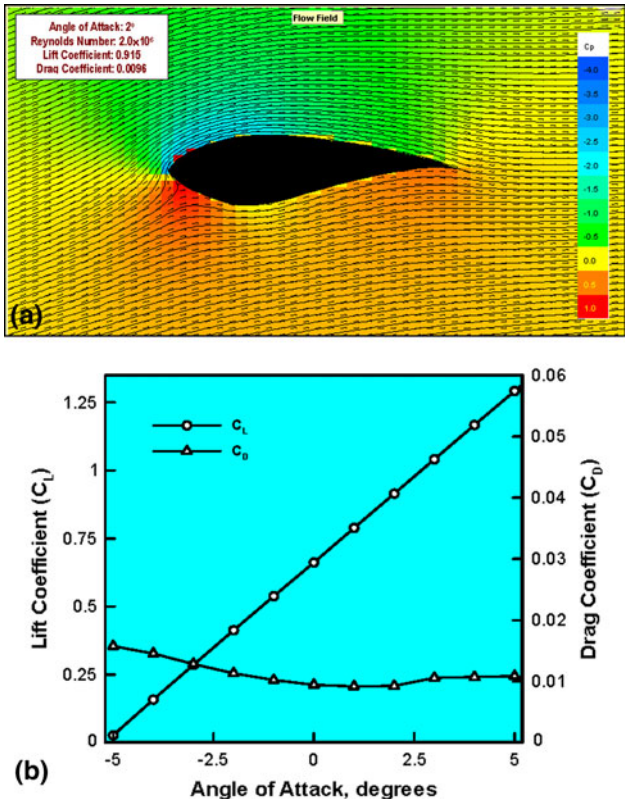

Fig. 6 An example of the Javafoil (Ref 8) results pertaining to (a) the two-dimensional distribution of the coefficient of pressure, Reynolds number and coefficients of lift and drag; (b) variation of the coefficients of lift and drag with the wind angle of attack

trailing-edge airfoil thickness variation along the span (edge-wise bending loads are most likely to cause failure of the trailing edge blade sections) are used as design variables. The blade mass (to be minimized) is used as an objective function while maximum allowable flap-wise bending strains, blade-tip deflections and a minimal edge-wise bending-controlled fatigue life of at least 20 years are used as constraints. Once, for a given aerodynamic design of the blade, the inner-level optimization has yielded the minimal blade mass, a cost assessment analysis is employed within the outer-level optimization loop.

Lastly, the outer-level optimization loop objective function, the CoE, is computed as a ratio of the blade material/production cost and the aforementioned AEP. This procedure is repeated until suitable objective function minima are found for both the outer-level and the inner-level optimization loops.

In the subsequent subsections of this section, a brief overview is provided of the aerodynamics-based AEP analysis, finite element-based structural analysis and a post-processing-based durability analysis employed within the current multi-disciplinary design optimization of a 5 MW HAWT blade.

2.2.1 Aerodynamics-Based Computational Analysis. The purpose of the aerodynamic analyses employed in the present work was two-fold:

(a) To determine pressure distribution over the blade surface which is needed in the determination of wind-based loading for the quasi-static structural and durability analyses of the blade.
(b) To compute the aerodynamic efficiency (as quantified by the AEP) for a given design of the blade.

Towards that end, two different aerodynamics codes were employed: (a) *Javafoil* (Ref 8) computer program, a two-dimensional aerodynamic analysis code which solves the flow equations over an airfoil by implementing the boundary integral method. For the given airfoil profile and size, the wind speed and the angle of attack, the program generates a distribution of pressures over the blade surface, calculates the Reynolds number and the corresponding lift and drag coefficients. An example of the results pertaining to the spatial distribution of the coefficient of pressure (a ratio of the pressure minus mean-stream pressure difference and the half product of mean-stream air-density and squared wind velocity) is displayed in Fig. 6(a). The corresponding wind angle of attack, the Reynolds number and the coefficients of lift and drag are also displayed in Fig. 6(a). In Fig. 6(b), Javafoil-generated results pertaining to the variation of the lift and drag coefficients with the wind angle of attack are displayed; and (b) the second aerodynamics-based code used in the present work was *PROPID* (Ref 9). This computer program utilizes user-supplied blade length and span-wise airfoil geometrical parameters (e.g. chord length and section thickness distributions, twist angle schedules, etc.) and the corresponding Javafoil aerodynamic results (e.g. Reynolds numbers with the associated angles of attack, lift and drag coefficients) to compute the variation of the aerodynamic efficiency parameter, α, with the blade Tip Speed Ratio, TSR (a ratio of the blade-tip peripheral velocity and the wind speed). This information is next combined with the user-provided input data pertaining to the hub-height, maximum allowable tip speed, cut-in wind velocity (the minimum wind speed required for the start-up of the wind turbine), cut-out wind speed (wind-speed at which the maximum system rating of the turbine is achieved) and wind turbine

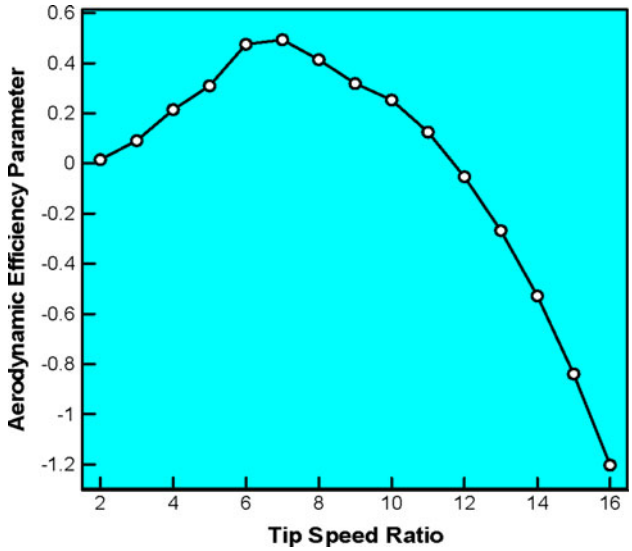

Fig. 7 An example of the PROPID (Ref 9) results pertaining to variation of the aerodynamic efficiency parameter of the rotor with the tip speed ratio

availability percentage to compute the AEP. An example of the typical results generated by PROPID is displayed in Fig. 7. This figure shows a variation of the aerodynamic efficiency parameter, α, with the blade TSR. It is seen that there is an optimal TSR at which α is maximum.

2.2.2 Finite Element-Based Structural Analysis. The HAWT blades are generally oriented in such a way that their wide faces are at a small angle relative to the rotation plane of the rotor while the wind direction is roughly normal to this plane. It should be recognized however that particularly in the case of long HAWT blades the peripheral velocity of the outermost sections of the blades could be several times higher than the typical wind speeds during normal operation of the turbine. Consequently, the effective wind direction as experienced by the HAWT blades varies along the span and in the case of outermost section of the blade is nearly parallel with the rotation plane of the rotor. To maximize the wind energy captured (i.e., the aerodynamic lift) by the blade in the presence of a variable wind direction along the span, the blades are typically twisted.

The aerodynamic lift mentioned above can be decomposed into two components: (a) a torque component which is parallel with the rotation plane of the rotor and causes the blade to spin and (b) a thrust component which gives rise to flap wise bending of the blades. It should be recognized that the lift-induced loading has both a persistent/static-like and a time-varying component (the latter one is due to natural variability of the wind). In addition, the relative fraction of the two load components changes during rotation of the rotor due to the wind-shear effects.

In addition to the lift-related loads discussed above, wind-turbine blades are also subjected to gravity loads. These loads are the highest in magnitude when the blade is in a nearly horizontal position and they cause edge-wise bending of the wind-turbine blade. Since the blades bend one way when they are on the right-hand side of the tower while they bend in the other direction when they are on the left-hand side of the tower; gravity loading also contains a variable component.

Wind turbine blades are also subjected to centrifugal loading due to rotation of the rotor. Nevertheless, since the upper-bound angular velocity of the rotor is typically in a 10-20 rpm range, centrifugal-tensile loads along the blade length are generally not considered as design-controlling/life-limiting loads (and are, hence, ignored in the present work).

Following the conventional practice, the mechanical/structural response of the HAWT blades subjected to the wind/gravity loading is analyzed separately in the cases of a sustained quasi-static loading and a time-dependent loading. In this section, only the case of the quasi-static loading is considered.

To determine the quasi-static structural response of the blade, a static finite-element analysis was carried out in which the root-edge of the blade was fixed and the blade outer surfaces subjected to a gust-induced loading (defined below). The results of this analysis were used to determine the turbine-blade bending strength (as measured by the largest tensile and compressive-signed equivalent strains within the interior load-bearing structures of the blade) and by the turbine-blade bending stiffness (as quantified by the average deflection of the blade tip). It should also be noted that since the wind-induced loading was found to be nearly proportional (i.e., the signed equivalent strain is found to scale with squared wind speed while the orientation of the in-plane principal coordinate system within the most highly stressed blade sections was found not to change significantly during loading), the results of the structural analysis were used also in the fatigue-life assessment analysis (discussed in next section). In other words, local strains are assumed to scale linearly with the level of local wind-induced loading so that the gust-based strains can be used to directly calculate the corresponding strains at any level of wind-induced loading.

To compute the wind-based loading for the given airfoil profile and size, the wind speed and the angle of attack, the *Javafoil* computational results pertaining to the distribution of pressure over the blade surface sections at 10 equally spaced span-wise stations are used. These results are next interpolated to obtain the pressure distribution (i.e., wind-based loading) over the entire blade surface.

For the quasi-static structural analysis, wind-based loads were derived by considering a 50-year extreme gust of 70 m/s (IEC Class 1 (Ref 10)). The blade is assumed to be in a fully *feathered* position (i.e. pitch of the blade is adjusted to obtain the wind attack-angle associated with the lowest aerodynamic loads). To attain the most conservative loading case, it was assumed that the gust-induced loading results in each blade section simultaneously reach their local maximum-lift coefficient condition.

As mentioned earlier, the present finite element analysis was also employed to determine the state of loading within the blade under the mean wind speed loading conditions. The mean wind speed was computed using the procedure outlined in Ref 4 and set equal to the Rayleigh wind speed at the hub height of the turbine. This procedure yielded a wind mean speed at the hub elevation of 8.6 m/s in the direction of rotor axis.

All the calculations pertaining to the structural response of the wind-turbine blade were done using ABAQUS/Standard, a commercially available general-purpose finite-element program (Ref 11).

2.2.3 Post-Processing Durability Analysis. It is well-established that in most cases the life cycle of a wind-turbine blade is controlled by its fatigue strength (in the presence of

local thermal and aggressive environmental conditions, e.g. Ref 3). While it is generally fairly straight forward to quantify fatigue strength of the structural materials (e.g. glass fiber reinforced polymer-matrix composites, in the case of wind-turbine blades analyzed in the present work) under constant-amplitude cyclic loading conditions, relating this strength to the durability of the component (a turbine blade, in the present case) is often quite challenging. This is primarily due to the fact that the turbine blades are subjected in-service to the non-constant amplitude cyclic loads. In other words, real time-varying wind-induced loading is irregular and stochastic and the associated load history affects the component fatigue life in complex ways. The procedure used in the present work to correlate the material fatigue strength with the component durability/life is based on the use of a cycle-counting algorithm (the so-called "*Rainflow*" cycle-counting analysis (Ref 12)), a linearized Goodman diagram (e.g. Ref 13) to account for the effect of mean-stress/strain on the material fatigue life/strength and the Miner's linear-superposition principle/rule (Ref 14). Since this procedure was described in great detail in our recent work (Ref 7), only a brief overview of its main components, i.e. the rainflow cycle counting analysis, the Goodman diagram and the Miner's rule, will be provided here.

Rainflow Analysis. When a time-varying load signal is recorded over a sampling period and needs to be described in terms of a three-dimensional histogram (each bin of which being characterized by a range of the signal amplitude and a range of the signal mean value), procedures like the rainflow counting algorithm are used. Within this procedure, the first step involves converting the original load signal into a sequence of load peaks and valleys. Then, the cycle counting algorithm is invoked. To help explain the rainflow cycle-counting algorithm, a simple load signal (after the peak/valley reconstruction) is depicted in Fig. 8(a), with the time axis running downward.

Within the rainflow cycle-counting algorithm, separate counting of load half-cycles is carried out for the ones starting from the peaks and the ones starting from the valleys. In Fig. 8(a), only the half-cycles originating from the peaks are analyzed. A half-cycle then starts from each peak and ends when one of the following three criteria is met:

(a) When the end of the signal is reached (case A in Fig. 8a).
(b) When the half-cycle in question runs into a half-cycle which originated earlier and which is associated with a higher peak value (case B in Fig. 8a).
(c) When the half-cycle in question runs into another half-cycle which originated at a later time and which is associated with a higher value of the peak (case C in Fig. 8a).

Once all the half-cycles are identified they are placed in bins, each bin being characterized by a range of the load amplitude and the load mean value. An example of the resulting three-dimensional histogram showing the number of cycles/half-cycles present in the load signal associated with a given combination of the load amplitude and the load mean-value is depicted in Fig. 8(b).

In accordance with our prior work reported in Ref 7, to account for the time-varying component of the wind-induced and gravity loading, the so-called WISPER (Wind Spectrum

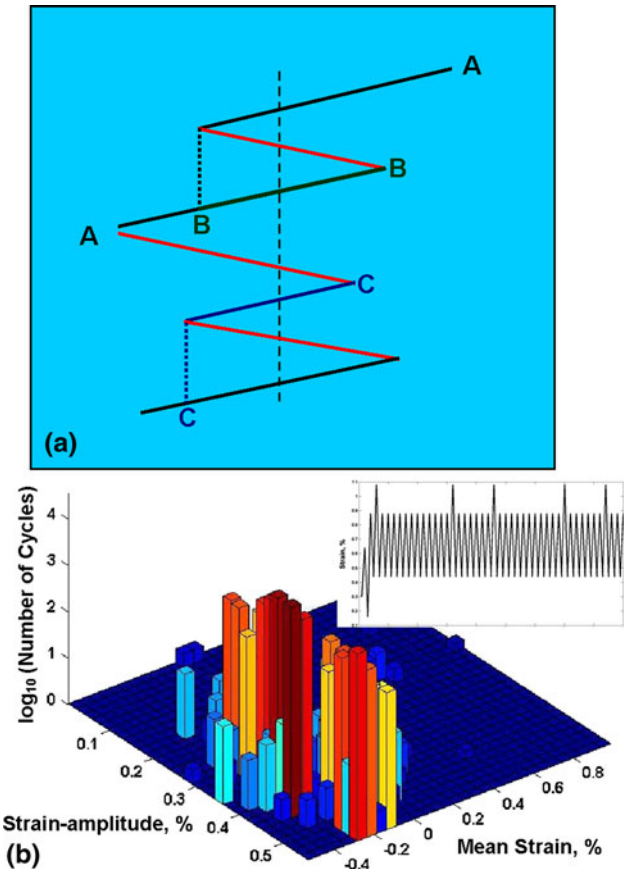

Fig. 8 (a) Application of the rainflow cycle-counting algorithm to a simple load signal after the peak/valley reconstruction. Please see text for explanation; (b) the resulting three-dimensional histogram showing the number of cycles/half-cycles in each mean stress/strain-stress/strain amplitude bin

Reference) loading history/profile (Ref 15) (a reference load spectrum typically used in the design of wind turbine blades in Europe) was used (after proper scaling). A short duration trace of this signal is displayed as an inset in Fig. 8(b).

Goodman Diagram. Before presenting the basics of the Goodman diagram, it is important to recognize that the fatigue life of a material is a function of both the stress/strain amplitude and the stress/strain mean value. Often, the stress/strain mean values are quantified in terms of an R-ratio which is a ratio of the algebraically minimum and the algebraically maximum stress/strain values (associated with the constant-amplitude cyclic-loading tests). From the definition of the mean stress/strain, it can be readily shown that fatigue-loading tests carried out under constant R-ratio conditions correspond to the tests in which the mean stress/strain scales with the corresponding amplitude. To construct the Goodman diagram, constant-R/constant-amplitude fatigue-test results are plotted, in a stress/strain amplitude versus stress/strain mean-value diagram. As depicted in Fig. 9(a), constant-R data fall onto a line emanating from the origin. In Fig. 9(a), $R = 0.1$ and $R = 0.5$ data are associated with a positive/tensile mean stress/strain value, $R = -1$ corresponds to a zero mean-value, while $R = 10$ and $R = 2$ pertain to a negative/compressive mean value.

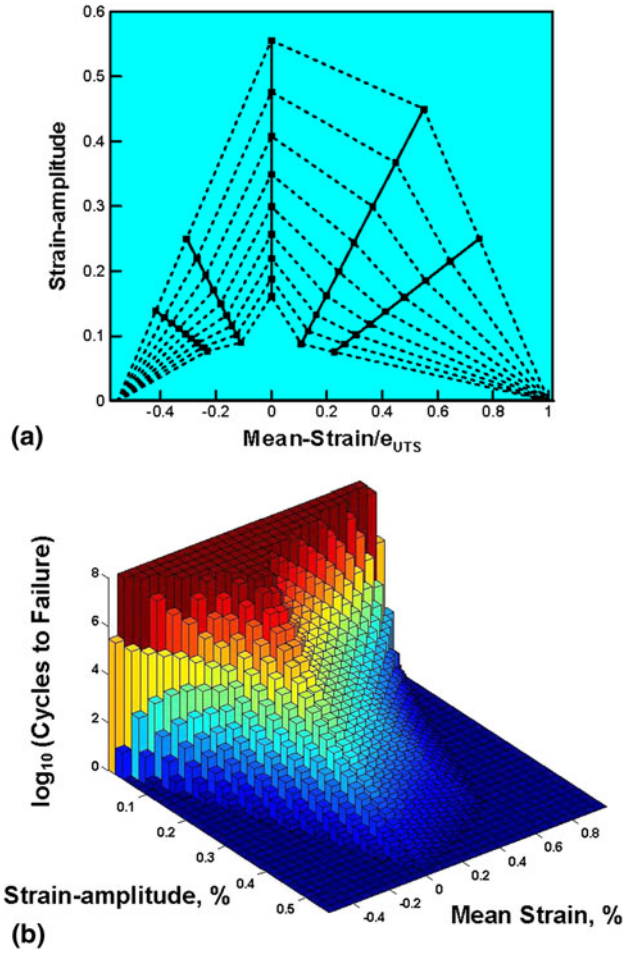

Fig. 9 An example of (a) Goodman diagram showing constant fatigue-life data (dashed lines) and constant R-radio data (the solid lines emanating from the origin); (b) the corresponding three-dimensional histogram showing the effect of stress/strain amplitude and the stress/strain mean-value of the material fatigue life

To construct the corresponding linearized Goodman diagram, constant fatigue-life data associated with different *R*-ratio values are connected using straight lines. To complete the construction of the Goodman diagram, the constant fatigue-life lines are connected to the ultimate tensile stress/strain and to the ultimate compressive stress/strain points located on the zero-amplitude horizontal axis. The completed Goodman diagram displayed in Fig. 9(a) then enables, through interpolation, determination of the fatigue life for any combination of the stress/strain amplitude and stress/strain mean value. Hence, a three-dimensional histogram similar to that one shown in Fig. 8(b) can be constructed except that the number of cycles here represents the total number of cycles to failure rather than the number of cycles in the analyzed load signal. An example of such three-dimensional histogram is displayed in Fig. 9(b).

Miner's Rule. The cycle counting procedure described earlier enables computation of the number of cycles/half-cycles in the given load signal which fall into bins of a three-dimensional histogram (Fig. 8b). The use of the Goodman diagram, on the other hand, enables the computation of a similar tri-dimensional histogram but for the number of cycles to failure (i.e. the fatigue life) (Fig. 9b). According to the Miner's rule, a ratio of the number of cycles and the corresponding total number of cycles, for a given combination of the stress/strain amplitude and stress/strain mean value, defines a fractional damage associated with this component of the loading. The total damage is then obtained by summing the fractional damages over all combinations of the stress/strain amplitude and the stress/strain mean value.

The total fatigue life under the given non-constant amplitude time-varying loading is obtained by dividing the load-signal duration by the total fractional damage. This procedure clearly postulates that fatigue failure corresponds to the condition when the total damage is equal to unity.

2.2.4 Material/Production Cost Analysis. Following the procedure described in Ref 4, a cost function was developed in order to compute materials/fabrication cost for the blades analyzed in the present work. The cost function included the following components:

(a) A cost sub-function for master blades and mold sets which assumes that the associated cost scales directly with surface area of the blade.
(b) A tooling cost sub-function which also assumes that the associated cost scales with the blade surface area but furthermore assumes that there is an added cost, due to reinforcement requirements, which scales with the blade length.
(c) The production cost sub-function which assumes that, for a mature blade fabrication process, the associated cost scales directly with the blade mass. This cost function further includes the so-called "*learning-curve*" effect. This effect is assumed to be cycle-controlled and the time it takes 100 cycles (i.e., 100 fabricated blades), before the production cost reaches its long-term level.
(d) These four components of the recurring production cost are complemented with a fixed-cost function which includes the cost of master blades, mold sets and tooling as well as a 10% interest rate.

3. Results and Discussion

As discussed in Sect 2, as part of the present work, a multi-disciplinary optimization procedure has been developed for use in the design of cost-effective glass-fiber reinforced epoxy-matrix composite 5 MW HAWT blades. Within this procedure, a computer program was developed which enables automated creation of fully parameterized geometrical and meshed models, as well as the generation of a complete finite-element input deck for a large single 5 MW HAWT blade. For a given choice of the airfoil shape, span-wise chord-length and twist-angle schedules, the program enables the optimization procedure to assign the lateral location of the shear webs, thickness for all aerodynamic (i.e. the outer skins) and structural (i.e. the shear webs and the spar caps) components and composite-laminate ply stacking for each component as a whole or for different portions of the same component. In addition, interfacing of the model-generation computer program with an aerodynamics analysis computer program (Ref 8) enabled automated generation of the sustained wind-based loading conditions. This was complimented by the addition of non-constant amplitude reference time-varying loading to construct

fairly realistic in-service loading conditions experienced by a large HAWT blade. The results obtained from the quasi-static finite element analyses of the HAWT-blade enabled not only investigation of the structural response of the blade (i.e. the extent of flap-wise bending and the extent of blade tip deflection, etc.), but also predictions of the HAWT-blade high-cycle fatigue controlled life cycle. In addition, this program enables the execution of a two-level optimization scheme. Within the outer-level optimization loop the blade shape is optimized with respect to its aerodynamic efficiency while within the inner-level loop the blade interior architecture is optimized with respect to its structural efficiency. The results of the two optimization routines are finally combined to assess the blade economics, i.e., the CoE.

Due to space limitations, only few representative results obtained in the present investigation will be shown and discussed in the following sections.

It should be noted that each portion of the present work included a mesh-convergence study to ensure that the finite-element mesh used was a good compromise between a computational accuracy and computational cost. The results of the mesh convergence studies will not be shown for brevity.

3.1 The Baseline Case

At the beginning of the present investigation, the procedure outlined in Ref 4 was followed in order to establish/construct a prototypical 5 MW HAWT-blade. The base-line case is based on the S818 airfoil-shape (Ref 4) (Fig. 3a), the primary structural member is a box-shape spar with (vertical) shear webs being located at distances equal to 15 and 50% of the section-chord length (as measured from the leading edge) and a substantial build-up in the spar cap thickness between the two vertical shear-webs. Examination of the HAWT-blade construction depicted in Fig. 3(a) suggests that due to a relatively large spar-cap width and laminate thickness, good edge-wise bending stiffness/strength is expected. This is however attained at the expense of the flap-wise bending stiffness/strength which could have been increased should the aft/right portion of the shear web had been placed in the section of the blade associated with the largest blade thickness.

A typical plan-form (Fig. 3b) is used in the baseline blade design. The plan-form shows the variation of the blade chord-length with a radial distance r from the hub rotation axis with R being the radial location of the blade tip, i.e., the rotor radius. Figure 3(b) shows that there is a linear taper from the maximum-chord section located at $r/R = 0.25$ to the blade tip ($r/R = 1.0$). The blade root is located at $r/R = 0.05$ and is circular in cross section. The cross section is assumed to remain circular up to $r/R = 0.07$ and thereafter undergoes a gradual transition to the pure airfoil section located at $r/R = 0.25$.

As mentioned earlier, HAWT-blades are commonly twisted. Consequently, the baseline-blade case analyzed here was given a twist along its length. Specifically, the airfoil sections located at $r/R = 0.25$, 0.5, 0.75 and 1.0 were twisted by 10°, 2.5°, 0°, and −0.5°, respectively.

The exterior airfoil skins and the interior vertical shear webs are constructed using a sandwich-like material consisting of (−45°/0°/45°) tri-axial fiber-glass composite-laminate face-sheets separated by a balsa-wood core. The spar caps are constructed of alternating equal-thickness layers of the tri-axial laminates (described above) and unidirectional laminates making the contribution of 0° laminate and the off-axis laminate 70 and 30%, respectively. A summary of the composite-laminate lay-up sequences and ply thicknesses used in different sections of the baseline HAWT-blade design is provided in Table 1.

As mentioned earlier, all composite laminates mentioned above were based on epoxy matrix reinforced with E-glass fibers. As far as the adhesive layers connecting the spar caps to the interior faces of the skins are concerned, they were taken to be epoxy based. A summary of the stiffness, mass and composite mixture properties (where applicable) of the materials used are provided in Table 2. In Table 2, *Tri*, *Uni* and *Mix* are used to denote respectively the tri-axial, uni-axial and the spar-cap mixture composite laminates.

3.1.1 Structural Response of the Baseline HAWT Blade. An example of the (flap-wise) structural response of the baseline HAWT blade when subjected to 70 m/s gust loading is displayed in Fig. 10(a). Since the interior shear-web/spar-cap substructure of the blade carries most of the flap-wise bending loads and hence its structural integrity is of primary concern, the outer skins are not displayed in Fig. 10(a). The results displayed in Fig. 10(a) reveal the spatial distribution of the equivalent strain over the interior substructure of the blade near

Table 1 HAWT-blade composite-laminate lay-up sequence

Layer number	Material	Thickness
Exterior skins and internal vertical shear-webs		
1	Gel coat	0.68 mm
2	Random-mat laminate	0.5 mm
3	Triaxial laminate	1.2 mm
4	Balsa core	0.005 × chord length
5	Triaxial laminate	1.2 mm
Spar-caps		
1	Triaxial laminate	1.2 mm
2	Uniaxial laminate	1.2 mm
Continued alternating layers of 1 and 2		

Table 2 Summary of the HAWT-blade material properties

Property	Uni	Tri	Mix	Random mat	Balsa	Gel coat	Epoxy adhesive
Axial Young's modulus, E_{xx}, GPa	31.0	24.2	27.1	9.65	2.07	3.44	2.76
Transverse Young's modulus, E_{yy}, GPa	7.59	8.97	8.35	9.65	2.07	3.44	2.76
In-plane shear modulus, G_{xy}, GPa	3.52	4.97	4.70	3.86	0.14	1.38	1.10
Poisson's ratio, v_{xy}	0.31	0.39	0.37	0.30	0.22	0.3	0.3
Fiber volume fraction, v_f	0.40	0.40	0.40	…	N/A	N/A	N/A
Fiber weight fraction w_f	0.61	0.61	0.61	…	N/A	N/A	N/A
Density, ρ, g/cm^3	1.70	1.70	1.70	1.67	0.l44	1.23	1.15

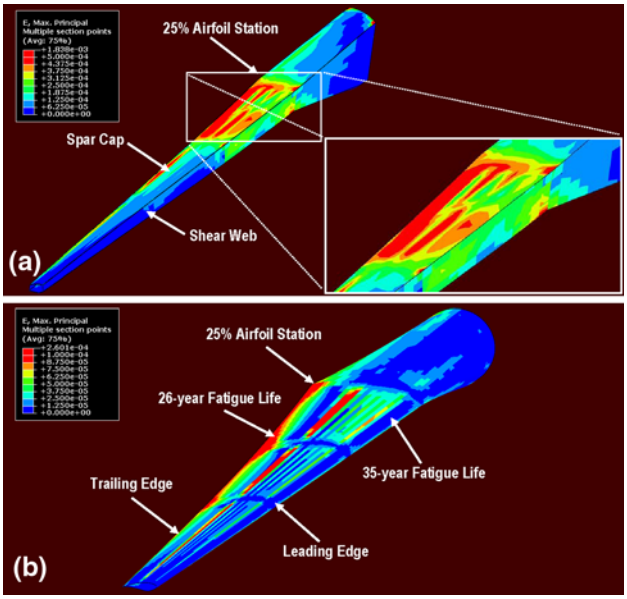

Fig. 10 (a) Equivalent strain distribution over the interior substructure caused by a 70 m/s gust; (b) equivalent strain distribution over the outer skin due to peak gravity loading for the baseline blade design

the 0.25R span station. These results pertain to the case when the blade is in the horizontal position; it is fixed at its root and subjected to the gravity loading and the aerodynamic forces resulting from pressure difference across the blade thickness under the gust-based loads.

The results displayed in Fig. 10(a) show that the maximum equivalent strains experienced by the spar caps at their tensile and compressive sides are 0.00184 and 0.00035, respectively. As mentioned earlier, the longitudinal spar is the key load-bearing member of the blade and any compromise in its structural integrity implies an imminent loss of the HAWT-blade functionality and its structural failure. Hence, it is critical to assess if the maximum strains displayed in Fig. 10(a) exceed the corresponding tensile and compressive material strengths (as quantified by the corresponding critical material strains). However, before one can proceed with assessment of the HAWT-blade safety factor under the imposed gust-based loading conditions, one must recognize that the effective strength of the blade material may be reduced relative to that found in the nominally same material when processed under normal material processing conditions and subjected to normal storage/handling practices.

In comparison to the standard materials-processing practice, the material in the HAWT-blade is generally fabricated under different conditions (i.e. the material is laid-up at the time when the blade is being manufactured) and is exposed to varying temperatures, ultraviolet-radiation, humidity, salinity, and other environmental conditions (and is, hence, expected to have undergone a considerable amount of degradation in its as-fabricated condition). To account for all these strength-degrading effects, the IEC 61400-1 standard (Ref 10) prescribes a set of so-called "*material partial safety*" factors. Following the procedure described in Ref 4, the overall/cumulative material strength-reduction factor was assessed as 2.9. Hence, for the prototypical 0.0220 and 0.0105 ultimate uniaxial tensile and ultimate uniaxial compressive strains (before they are corrected using the material partial safety factors) for the E-glass/epoxy composites used in the present work, the smallest safety factors (defined as a ratio of the corrected ultimate strains and the corresponding observed maximum equivalent strains) are estimated as 0.0220/2.9/0.00184 (= 4.1) and 0.0105/2.9/0.00035 (= 10.3) for the tensile and compressive sections of the spar caps, respectively. Since these safety factors are larger than 1.0, the baseline blade design appears not to be static-strength critical.

The blade tip deflection determined as part of the present quasi-static structural analysis was found to be ca. 7.5 m. Since this value exceeds a commonly recommended maximum allowable value of $0.1 \times R = 6.0$ m, the baseline blade design appears to be stiffness critical. As discussed earlier, an excessive blade-tip deflection is of major concern in the case of upwind turbines since it might lead to a collision of the blade with the wind-turbine tower.

3.1.2 Fatigue Life of the Baseline HAWT Blade. As mentioned earlier, the so-called "*proportional loading*" case was adopted in the present work according to which strains scale directly with the load magnitude and the orientation of their principal components remains unchanged with a change in the load magnitude. The proportional loading assumption simply implies that there is a frequency component in the wind-based loading which is equal to the gravity-loading frequency. Hence, the strain state in the blade at any instant can be calculated by simply scaling down the wind loading-induced strains obtained in the previous section (Fig. 10a) by a factor of $\left(70/V^2_{\text{wind}}\ \text{m/s}\right)^2$ where V_{wind} is the instantaneous wind speed and by adding the effect of gravity loading. It should be noted that, before the fatigue life assessment procedure based on the rain flow cycle counting algorithm, the Goodman diagram and the Miner's rule can be applied, the issue of multi-dimensional strain state within different sections of the HAWT-blade have to be addressed. While in metallic materials the time-varying compressive strains are not generally harmful, composite materials (due to the potential for fiber micro-buckling) are generally quite susceptible to laminate in-plane compressive strains. To provide a fairly conservative assessment of the baseline HAWT-blade fatigue life and take into account the effect of compressive strains, the strain multi-axiality is handled through the use of a "*signed*" equivalent strain. That is, the entire stress/strain state is assumed to be quantified by the equivalent strain to which a sign is attached consistent with the sign of the largest (by magnitude) principal strains.

As mentioned earlier, time-varying component of the wind-induced loading is modeled by the WISPER load signal. While scaling this load signal (whose values range between 1 and 64 with the level of 25 corresponding to a zero load), the WISPER mean value (32) was assumed to correspond to the previously computed wind mean speed of 8.6 m/s.

An example of the results pertaining to the fatigue life assessment for the baseline HAWT blade is displayed in Fig. 10(b). Since the blade fatigue life is controlled by edge-wise bending loads, the sections of the blade most prone to fatigue-based failure are commonly found along the trailing edge (and typically near the 0.25R span-section). These sections are part of the outer skin and, in contrast to Fig. 10(a), the outer skins of the blade are displayed in Fig. 10(b). The results displayed in Fig. 10(b) show the fatigue life (in years) for different sections of the blade in the vicinity of the 0.25R span station, where the values of the fatigue life are the lowest. Since the fatigue life everywhere in the blade exceeds the

required level of 20 years, the baseline blade design appears not to be fatigue critical.

3.2 The Optimized Blade Design

The multidisciplinary procedure described in Sect 2 yielded the following optimal design of the 5 MW HAWT blade:

(a) *Chord-length schedule*: 5.43 m at r/R = 0.25, 4.21 m at r/R = 0.50, 2.99 m at r/R = 0.75 and 1.77 m at r/R = 1.0.
(b) *The twist angle schedule*: 10.8° at r/R = 0.25, 2.8° at r/R = 0.50, 0° at r/R = 0.75 and −0.7° at r/R = 1.0.
(c) *Blade mass*: 29,553 kg (the baseline case blade mass was 26,122 kg).

The progress of the optimization procedure is displayed in Fig. 11(a) and (b). These figures display the variations of the blade mass and the AEP, Fig. 11(a) and the CoE, Fig. 11(b), within the outer-level optimization loop iteration number.

3.2.1 Structural Response of the Optimized HAWT Blade. The (flap-wise) structural response of the optimized HAWT blade when subjected to 70 m/s gust loading is displayed in Fig. 12(a). The results displayed in Fig. 12(a) reveal the spatial distribution of the equivalent strain over the interior substructure of the blade near the 0.25R span station. These results again pertain to the case when the blade is in the horizontal position; it is fixed at its root and subjected to the gravity loading and the aerodynamic forces resulting from pressure difference across the blade thickness under the gust-based loads.

The results displayed in Fig. 12(a) show that the maximum equivalent strains experienced by the spar caps at their tensile and compressive sides are 0.0015 and 0.00075, respectively. Following the procedure described in Sect 3.1.1, the following values of the quasi-static structural safety factors were respectively obtained for the spar cap sections experiencing the largest (by magnitude) tensile and compressive equivalent strains: 0.0220/2.9/0.0015 (= 5.05) and 0.0105/2.9/0.00075 (= 4.82). Based on these findings it can be concluded that the optimized blade design is not static-strength critical.

The blade tip deflection determined as part of the present quasi-static structural analysis was found to be ca. 6.6 m. Since this value exceeds a commonly recommended maximum allowable value of 0.1 * R = 6.0 m, the optimized blade design, while superior to the baseline design, is still stiffness critical.

3.2.2 Fatigue Life of the Optimized HAWT Blade. The results pertaining to the fatigue life assessment for the optimized HAWT blade are displayed in Fig. 12(b). The results displayed in Fig. 12(b) show that the fatigue life (in years) of some of the outer shell sections near the trailing edge has dropped to 20 years. This finding suggests that the optimized blade design is at the verge of becoming fatigue critical.

3.2.3 A Brief Discussion on the Optimized Blade Design. The structural performance and fatigue/durability results presented in Fig. 12(a) and (b), and the corresponding blade-tip deflection results for the optimized blade design

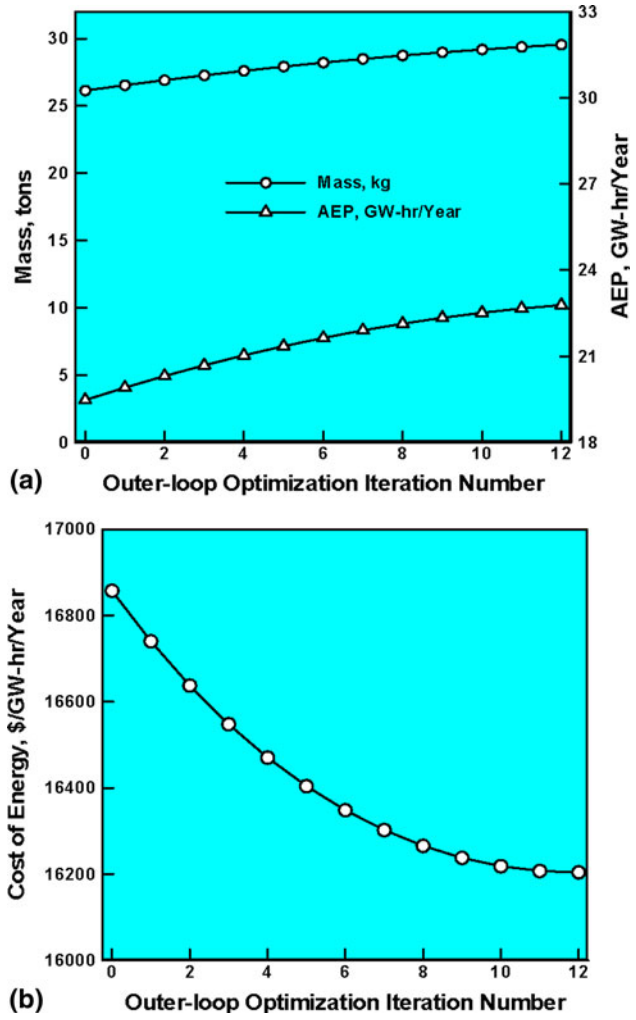

Fig. 11 Evolution of the blade design with the outer-level optimization loop iteration number: (a) blade mass and the AEP; (b) the CoE

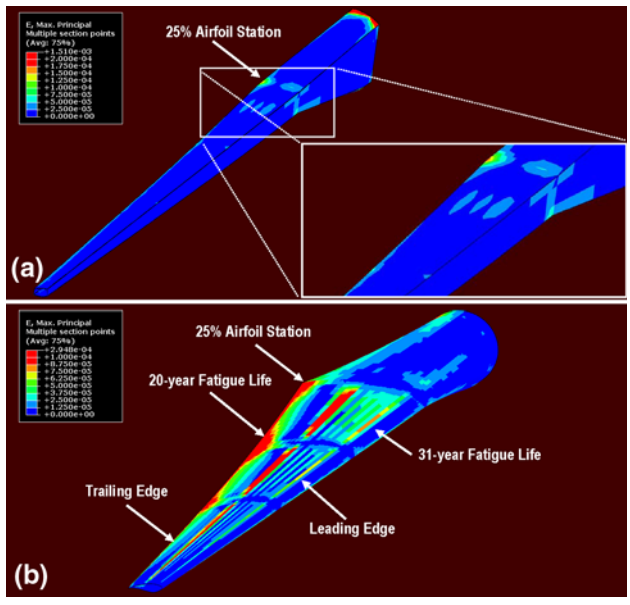

Fig. 12 (a) Equivalent strain distribution over the interior substructure caused by a 70 m/s gust; (b) equivalent strain distribution over the outer skin due to peak gravity loading for the optimized blade design

clearly revealed the challenges associated with the development of cost-effective large HAWT blades. The main lessons learned in the present investigation can be summarized as follows:

(a) As long as the airfoil shape is retained (i.e., the blade thickness to chord length ratio is maintained constant), the chord-wise positions of the shear webs kept unchanged and the same type of glass-fiber reinforced composite laminate is used, it is impossible to simultaneously satisfy the quasi-static strength, fatigue-controlled durability and the blade stiffness functional requirements.
(b) While an increase in the spar-cap thickness used in the optimized blade design yielded an improved blade stiffness, this method of stiffness enhancement was not very mass-efficient since the added spar-cap mass was located closer to the flap-wise bending neutral axis.
(c) The added spar-cap mass leads to a degradation in the edge-wise fatigue strength of the blade due to an associated increase in the gravity loading.
(d) One of the possible ways of eliminating stiffness deficiency of the optimized blade is to increase the blade thickness. This can, however, result in a lower aerodynamic efficiency of the rotor and compromise static strength of the blade (the fibers farthest away from the flap-wise bending neutral axis will experience larger strains).
(e) Repositioning of the shear webs so that they are located in the region of the blade associated with the largest thickness is another potential stiffness improvement solution. It must be noted, however, that this may lead to larger edge-wise bending strains and to a lower fatigue life.
(f) Lastly, the use of higher stiffness laminates, e.g., carbon-reinforced composites or carbon/fiber-glass hybrid composites, is yet another remedy for the observed inferior stiffness of the optimized HAWT blade. However, these materials are inherently more expensive and fabrication of the blades may be associated with a higher production and tooling costs.

In our future communication, an attempt will be made to further improve the performance of the optimized 5 MW HAWT blade by examining quantitatively the effects of a larger blade thickness, alternative locations of the shear webs and the use of higher-stiffness composite laminates.

4. Summary and Conclusions

Based on the results obtained in the present work, the following main summary remarks and conclusions can be drawn:

1. A multi-disciplinary design-optimization procedure (based on the use of aerodynamic, structural, durability and cost computational analyses) has been developed for use in the design of HAWT blades.
2. The procedure is next utilized in order to optimize the design of a 5 MW HAWT blade whose length is ca. 60 m and mass of ca. 26 tons.
3. A special attention was given to the problem of developing wind and gravity-based (sustained and time-varying) loading conditions so that the structural performance and longevity of the blade can be assessed under conditions which fairly realistically mimic the in-service loading conditions.
4. This procedure clearly revealed the challenges associated with the development of cost-effective large wind turbine blades, which have to satisfy conflicting requirements pertaining to their aerodynamic efficiency, structural performance/reliability and fatigue-controlled durability.
5. Several potential solutions for remedying the performance deficiencies of the blade were identified and their shortcomings briefly discussed.

Acknowledgments

The material presented in this paper is based on work supported by a research contract with the Automotive Research Center (ARC) at the University of Michigan and TARDEC. The authors are indebted to Professor Georges Fadel for the support and a continuing interest in the present work.

References

1. 20% Wind Energy by 2030, Increasing Wind Energy's Contribution to U.S. Electricity Supply, DOE/GO-102008-2567, July 2008. http://www.osti.gov/bridge
2. D.A. Griffin, Evaluation of Design Concepts for Adaptive Wind Turbine Blades, SAND2004-2424, Sandia National Laboratories, 2002
3. P. Brondsted, H. Lilholt, and A. Lystrup, Composite Materials for Wind Power Turbine Blades, *Annu. Rev. Mater. Res.*, 2005, **35**, p 505–538
4. D.A. Griffin, WindPact Turbine Design Scaling Studies Technical Area-1-Composite Blades for 80- to 120-Meter Rotor, NREL/SR-500-29492, NREL, Washington, 2001
5. M. Grujicic, V. Sellappan, G. Arakere, J.C. Zeigert, K.Y. Kocer, and D. Schmueser, Multi-Disciplinary Design Optimization of a Composite Car Door for Structural Performance, NVH, Crashworthiness, Durability and Manufacturability, *Multidis. Model. Mater. Struct.*, 2009, **5**, p 1–28
6. MATLAB, *The Language of Technical Computing*, 7th ed., The MathWorks Inc., MA, 2006
7. M. Grujicic, G. Arakere, E. Subramanian, V. Sellappan, A. Vallejo, and M. Ozen, Structural-Response Analysis, Fatigue-Life Prediction, and Material Selection for 1 MW Horizontal-Axis Wind-Turbine Blades, *J. Mater. Eng. Perform.*, 2009. doi:10.1007/s11665-009-9558-8
8. M. Hepperle, *JavaFoil Users Manual*, 2005. http://www.mh-aerotools.de/airfoils/javafoil.htm
9. M.S. Selig and J.L. Tangler, A Multipoint Inverse Design Method for Horizontal Axis Wind Turbines, *AWEA Windpower Conference*, Minneapolis, MN, 2004
10. IEC-61400-3 (2009-02) Wind Turbines—Part 3, *Design Requirements for Offshore Wind Turbines Maintenance Result Date*, p 201
11. ABAQUS/Standard Version 6.8-1, User Documentation, Dassault Systemes, 2008
12. M. Matsuiski and T. Endo, Fatigue of Metals Subjected to Varying Stress, *Japan Soc. Mech. Eng.*, 1969
13. J. Goodman, *Mechanics Applied to Engineering*, Longman, Green, & Co, London, 1899
14. M.A. Miner, Cumulative Damage in Fatigue, *J. Appl. Mech.*, 1945, **12**, p A159–A164
15. A.A. Ten Have, WISPER and WISPERX: Final Definition of Two Standardized Fatigue Loading Sequences for Wind Turbine Blades, NLR-TP-91476U, National Aerospace Laboratory NLR, Amsterdam, The Netherlands, 1992